Atlantic Journal of Life Sciences
Volume 2025, Article ID 48, pages 13
https://doi.org/10.71005/292yr652

Original research

Computational Investigation of Triphenylmethane Acidic Dye for Textile Applications Using DFT and TDDFT Methods

Unsa Maqbool[1], Zunaira Rahat Gill[2], Nooria Fatima[1], Muqadas Majeed[1], Hamid Mehmood[1], Shagufta Nawaz[1], Hafsa Amjad[3], Sidra Ghafoor[4], Saira Najam[1], Muhammad Suleman[1], Majid Ali[1]

[1]Department of Chemistry, Riphah International University, Faisalabad campus, Faisalabad, Pakistan| [2]Department of Chemistry, University of Education Lahore, Faisalabad campus, Pakistan | [3]Department of Chemistry, University of Sialkot, Sialkot, Pakistan | [4]Department of Chemistry and Chemical Engineering, Shandong University, Jinan, China

Correspondence should be addressed to Majid Ali; Majid.ali@riphahfsd.edu.pk

Received: 31 August 2025; Revised: 12 September 2025; Accepted: 5 November 2025; Published 4 December 2025

KEYWORDS

Density Functional Theory (DFT), Acidic dye
Solvent effects
Electronic properties
UV-Vis spectroscopy
Textile applications

ABSTRACT

A comprehensive computational investigation of a triphenylmethane-acidic dye using Density Functional Theory (DFT) and Time-Dependent DFT (TDDFT) at the B3LYP/6-31G(d) level was conducted. The basic goal was to interpret the properties, i.e., structural, electronic, and spectroscopic properties in several media (gaseous, aqueous, and acetic acid) and to evaluate the suitability for textile applications. The geometric optimization of the acidic dye under observation undergoes solvent-induced changes, with the contraction of bond length (e.g., C1–C2 shortened from 1.4039 Å in gas to 1.3872 Å in water) and the angular variation of bonds (e.g., C2–C1–C6 decreased from 120.67° to 120.59° in ethanol), depicting the high conformational stability in polar solvents. The TD-DFT simulations showed a bathochromic shift and a high molar absorptivity (λmax ~245 nm, absorbance ~3200), indicating UV absorption in aqueous environments. The oscillator strength of strong π→π* electronic transitions in the 240–250 nm range further confirms the conjugated system's ability to interact effectively with light, an essential characteristic for dye brilliance and intensity on textile substrates. HOMO–LUMO analysis showed a solvent-dependent narrowing of the energy gap (ΔE), from 3.82 eV in the gas phase to slightly reduced values in ethanol and water, facilitating intramolecular charge transfer and favorable dye–fiber interactions. Mulliken population analysis and molecular electrostatic potential (MEP) mapping highlighted nucleophilic and electrophilic regions, consistent with expected binding behavior to textile fibers in solvents. IR vibrational analysis confirmed structural consistency across 700–3500 cm^{-1} in interaction with solvents. These findings show that solvent polarity significantly affects the dye's electronic structure and spectroscopic response, providing critical insights for its application in water-based or ethanol-assisted textile processing. The study affirms the value of DFT/TDDFT modeling for pre-screening dye candidates, enabling more efficient, cost-effective, and targeted dye design for optimal textile performance.

1. Introduction

Triarylmethane dyes are anthropogenic organic dyes with a backbone structure derived from triphenylmethane. These dyes are commonly used for dyeing textiles such as wool, silk, cotton, and leather (Chattopadhyay, 2011). This field of textile dyes, along with its chemistry, has advanced significantly and become more efficient through computational approaches, particularly Density Functional Theory (DFT) and Time-Dependent Density Functional Theory (TDDFT) (Bejan, Constantin, & Damaceanu, 2024). The dyes, such as triphenylmethane and its derivatives, are widely used on a large scale in the dying of protein-based fibers like wool and silk because of their affinity for acidic environments (Chavan, 2011a). Basically, improvements in acid dyes with specific features have led to a deep investigation of their structures and derivatives using quantum chemical methods. Specific features, such as light fastness, brightness, and stability, have played a pivotal role in this textile industry (Sekar, 2011). Density Functional Theory (DFT) and Time-Dependent Density Functional Theory (TDDFT) are two primary methods used to perform all calculations on the synthesized triphenylmethane-based acid dye (Choudhary, Patil, & Sekar, 2015). The result in the form of calculations has been obtained. These calculations involve comparing theoretical spectroscopic data, such as FT-IR and UV-Visible spectra, with experimental values to evaluate the structural and electronic features of the acid-dye molecule under observation (Amat, Miliani, Romani, & Fantacci, 2015). This comparative research approach increased the durability and reliability of computational modeling and provided valuable insights into the dye's reactivity, electronic transitions, and molecular interactions (El-Shafei, Hinks, & Freeman, 2011). Such studies are instrumental in understanding the structure-property relationships of acid dyes and play a pivotal role in designing and optimizing new dye candidates for advanced textile applications (Richards, 2012). Theoretical studies allow insights into dye-fiber interactions, reactivity indices, electron distributions, and spectroscopic behavior—factors critical for improving dye performance and minimizing environmental impact (Improta & Barone, 2012; Xie, Xia, Liu, & Cui, 2015). This study aims to evaluate a synthesized triphenylmethane acid dye using DFT and TD-DFT calculations, providing a detailed vision into its structural, electronic, and optical characteristics (Ripoche, 2015). The TPM dyes usually

exhibit charge-transfer excitations; range-separated functionals, such as CAM-B3LYP, are preferred over conventional hybrids, such as B3LYP, for TD-DFT calculations. The fundamental core structure of an acid dye, a TPM, is illustrated in Figure 1.

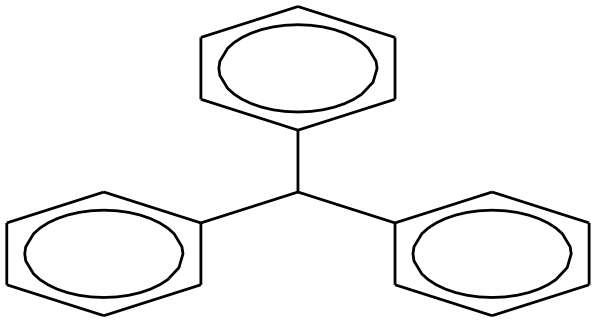

Figure 1: Structure of Triphenylmethane

2. Materials and Methods

All quantum-chemical calculations were performed using Gaussian 09 and visualized with GaussView 6. The structure of the synthesized triphenylmethane acid dye was optimized using DFT at the B3LYP/6-311+G(d,p) level (Ripoche, 2015). The two programs used for the computational calculations of the dye are the Gaussian 09 suite, and the structure visualization is obtained with Gauss View 06 (Deshmukh & Sekar, 2013). The dye is analyzed with different solvents (water and ethanol) using the PCM (IEFPCM) solvation model, and the frequency analyses are also performed. The frequencies are determined by the absence of imaginary frequency boundaries at B3LYP/6-311+G(d,p). To obtain the UV-Visible absorption spectra and identify the absorption peak, TD-DFT (TD-B3LYP/6-311+G(d,p)) calculations were performed on the basis set to ensure validity. This observation also provides information on the dye's excitation energies and levels (Oprea, Panait, Cimpoesu, Ferbinteanu, & Gîrţu, 2013). The charge distribution analysis has been conducted to interpret the HOMO-LUMO energy gaps and the Mulliken charges as MEP. The MEP surfaces were generated using Multiwfn and displayed in PyMOL. The FT-IR is also used to calculate the vibrational stimulations (Ebrahimi, Hadi, Abdulnabi, & Bolandnazar, 2014). A convergence criterion was fixed to Gaussian defaults. Solvent effects were treated using the integral equation formalism polarizable continuum model (IEF-PCM), with dielectric constants ε = 78.4 (water) and ε = 24.3 (ethanol). Frequency scaling factor 0.96 was applied. Optimized Cartesian coordinates and vibrational data are provided in the Supporting Information.

Computational chemistry techniques and programs were used to conduct a thorough analysis of the acid dye, yielding both experimental and theoretical calculations. The programs used for the calculations were Gaussian 09W and HyperChem 8, with DFT calculations carried out at the B3LYP and M06-2X levels using the 6-31G(d) and cc-pVDZ basis sets to interpret the dye optimization, molecular level modeling, geometrical optimization, and vibrational analysis (Geies, Gomaa, Ibrahim, Al-Hossainy, & Abdelwadoud, 2023). The absorption peak obtained through UV-Vis spectra, IR spectra obtained and these spectroscopic properties were studied and stimulated and then compared with the experimental and theoretical data to evaluate and validate the dye structural data (De Meyer, 2016; Laurent, Adamo, & Jacquemin, 2014) the charge distribution on the surface of dye and the reactivity points or receptors indicated were evaluated to understand the dye stability (Yaman, İpek Dirin, Kaplan, Seferoğlu, & Seferoğlu, 2022). The IR spectra obtained were also used to interpret the dye's electrical and molecular interactions and behavior. Meanwhile, the vibrational frequencies have also been calculated and evaluated (Sims, Abbott, Cowling, Goodby, & Moore, 2016). However, GaussView, PyMOL, and Multiwfn were used for visualization and wave-function analyses (De Meyer, 2016). The computational tools played a pivotal role in the structural, spectroscopic, and reactive behavior of the synthesized acid dye, supporting its high potential towards the textile industry and optoelectronic applications (De Meyer, Hemelsoet, Van Speybroeck, & De Clerck, 2014). The computational methods used in this study are given in Table 1.

Table 1: Computational methods used

	Steps	Calculations	Functional	Software	Purpose
1.	Geometry optimization	Ground state	B3LYP/6-311+G(d,p)	Gaussian 09	Optimized geometry
2.	Frequency analysis	Vibrational modes	B3LYP/6-311+G(d,p)	Gaussian 09	Confirms minima (no imaginary frequency)
3.	TD-DFT	Electronic excitations	TD-B3LYP/6-311+G(d,p)	Gaussian 09	Compute λ-max oscillator strength
4.	Solvent Modeling	PCM	IEFPCM	Gaussian 09	Solvent effects
5.	Charge analysis	Mulliken	-	Gaussian / Multiwfn	Charge distribution
6.	Visualization	MEP, MO plots	-	Multiwfn+PyMOL	Figures for manuscript

3. Results and Discussion

3.1. Molecular Geometry and Optimization

The geometrically optimized structure of the synthesized acid dye displayed a uniform, symmetrical structure, along with an electronic distribution (Bendjabeur, Zouaghi, Zouchoune, & Sehili, 2018). The computed bond lengths and bond angles were also analyzed using the acid dye triphenylmethane. As a result, the observed values were consistent with the standard values for the derivatives, confirming the dye's stability. The acid dye's structural, electrical, and spectroscopic properties greatly influenced the presence and polarity of the solvents used. The solvents significantly impact the dye behavior. The solvents used can alter the spectroscopic properties on interaction (Bendjabeur et al., 2018). However, solvents such as ethanol and water caused measurable changes in energy levels, surface charge distribution, bond lengths, and bond angles (El Alamy, Bourass, Amine, Hamidi, & Bouachrine, 2017). The solvents having polarity tend to have more impact to slightly compress bond lengths due to enhanced solute solvent electrostatic interactions, mainly stabilizing the dye's conformation and potentially improving its dyeing behavior. This also provides greater potential for the use of acid dyes in textiles (Gawale, Jadhav, & Sekar, 2018). The optimized 3D structure of the acid dye, TPM, along with the consistent atom numbering used in this study, is shown in Figure 2.

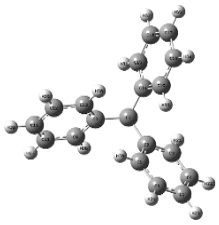

Figure 2: Optimized 3D molecular structure of the triphenylmethane acid dye showing standard atom numbering at the B3LYP/6-311+G(d,p) level.

3.2. Bond Length (Å)

The computed values obtained using computational tools were consistent with the standard bond lengths and angles of triphenylmethane, indicating the dye's stability. The table depicted a comprehensive comparison of the C–C and C–H bond lengths across different solvent media. For example, the C1–C2 bond was calculated to be 1.4039 Å in the gas phase, which shortened slightly in water Table 2 presents a comparative analysis of the calculated bond lengths of triphenylmethane under three alternative environments, such as the gas phase, water, and ethanol, with the help of DFT/B3LYP/6-3+G(d) and reference computed MP2 values. The obtained data indicate that the solvent exerts a slight but consistent effect on the molecule's geometry. The optimized geometric structure has delivered many practical, long-term benefits for the textile industry. Currently, the conjugation system, as evidenced by the shortened C–C bonds in polar solvents, results in brighter, more intense shades with improved light fastness. These enhanced dye properties in textiles play a vital role in ensuring that dyed textiles maintain color vibrancy over repeated use and laundering.

However, the interactions between C7–C8 and C14–C19 provide chemically reactive sites that can be tailored with functional substituents, thereby improving dye solubility, diffusion, and binding efficiency on both natural (e.g., cotton, wool) and synthetic (e.g., polyester, nylon) fibers. The solvent sensitivity of these bonds also enables optimization of dye performance for specific dyeing media. This also provides a pathway towards industrial dye processing. The bond-length analysis primarily contributes to the development of dye sensitivity and sustainable dyes. For example, dyes designed with structurally responsive bonds can adapt to environmental conditions such as pH, temperature, or light, opening pathways for thermo-chromic or photo-chromic textiles. Ultimately, a deep, detailed understanding of molecular geometry can help in synthesizing eco-friendly, sustainable dyes with improved biodegradability and reduced environmental impact. The study of acid dyes and their behavior in various solvents aligns with global trends toward green chemistry in the textile industry. So, the fine-tuning of bond lengths is not only fundamental to current dye performance but also pivotal in advancing future textile technologies. Figure 2 shows the complete computed calculations.

(1.3872 Å) and ethanol (1.387 Å), and closely aligned with MP2 values, indicating the dye's sensitivity to solvent effects. The polarity of water and ethanol affects the dye structure and bond length, and it was studied. The significant influence of solvents, particularly water and ethanol, on molecular geometry is evident from the computed bond angles and bond lengths. The continued consistency of the standard values studied for triphenylmethane demonstrated the conformational integrity. Meanwhile, the solvents used, such as water and ethanol, displayed stabilization in solute solvent interactions due to polarity and slight contractions in critical C-C bonds (Richards, 2012).

The physicochemical behavior of dyes is determined by measuring the bond length of the dye when it is applied to substrates. The bonds C1–C2, C2–C3, and C3–C4 are part of the aromatic conjugated system, and their slight shortening of bond lengths in polar solvents such as water and ethanol suggests enhanced π-electron delocalization. This suggests the stability of the chromophore, enhanced color strength, and shows restraint towards photo degradation. These mentioned features are highly desirable in the textile industry for dyes. Hence, the bonds like C4–C5 and C8–C13 further showed the conjugation pathway, affecting the bathochromic shift - a red shift in absorption that deepens dye color, making the dye more vivid and attractive on fabrics.

The C7–C8 and C14–C19 bonds serve as cross-ref bridges between the chromophoric core and any other functional groups present. The slight sensitivity of dye towards the polar solvents indicated the enhanced tuning of solubility and dye fiber interactions (Odoemelam, Emeh, & Eddy, 2018). The interactions between dyes and solvents are pivotal for proper dye diffusion and fixation on textile fibers, especially in aqueous or alcoholic dye baths. Moreover, bonds such as C7–H25, though small, influence the dye's polarity and hydrophilicity, thereby affecting how effectively the dye impregnates the fiber pores and forms van der Waals or hydrogen-bond interactions with the fiber surface. Overall, the observed changes in bond lengths across different solvent conditions not only reflect the dye's intrinsic flexibility but also hint at an optimized molecular geometry for maximum textile performance. These structural insights are vital for guiding the rational design of new dyes with superior application characteristics such as enhanced fastness, solubility, and fiber affinity (S. Shinde & Sekar, 2019). The optimized geometrical parameters reveal solvent-induced bond contractions and angular distortions, confirming the dye's stability in polar media.
The optimized geometrical parameters, along with comparative bond length data for the gas, water, and ethanol phases, are summarized in Table 2.

Table 2: A comparison of bond lengths determined in the gas phase and under various solvent conditions using DFT/B3LYP and Reference computed MP2 values, using the DFT/B3LYP/6-31G(d) basis set

Bond lengths (A°)						
		Computed bond lengths		Reference computed MP2		values.
Parameters	Gaseous phase	Water phase	Ethanol phase	Gas phase	Water phase	Ethanol phase
C1-C2	1.4039	1.3872	1.387	1.4039	1.3872	1.387
C2-C3	1.4067	1.3906	1.3905	1.4067	1.3906	1.3905
C3-C4	1.3976	1.3833	1.3831	1.3976	1.3833	1.3831
C4-C5	1.4007	1.3861	1.3861	1.4007	1.3861	1.3861
C7-C8	1.5359	1.5315	1.5315	1.5359	1.5315	1.5315
C7-H25	1.0993	1.0841	1.0844	1.0993	1.0841	1.0844
C8-C13	1.404	1.3872	1.387	1.404	1.3872	1.387
C14-C15	1.4066	1.3905	1.3909	1.4066	1.3905	1.3909
C14-C19	1.4041	1.3872	1.3865	1.4041	1.3872	1.3865

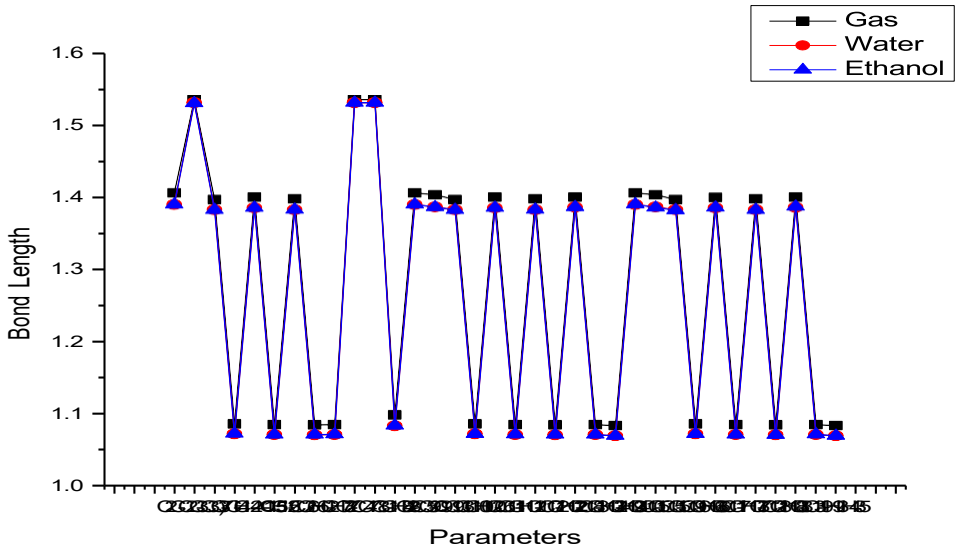

Figure 2: Computed bond lengths (Å) of triphenylmethane acidic dye obtained in gas phase optimization and PCM solvent models (water, ethanol).

The observed solvation effects on the acid dye and its stabilization can be further enhanced by increasing electron delocalization and compacting the bond framework. Notably, the central carbon (C7) is bonded to the three phenyl rings, which maintain relatively constant bond lengths across all solvent media, around 1.5359 Å in gas and 1.5315 Å in solvents, indicating lesser distortion at the molecular core. The agreement between DFT and MP2 results further validates the reliability of the DFT/B3LYP method for predicting solvent-dependent structural modifications. However, these validations emphasize that polar solvents such as water and ethanol produce slight but systematic decreases in bond lengths, reflecting stronger intermolecular interactions and solute stabilization, which could significantly impact the compound's reactivity and photo-physical behavior.

3.3. Frontier Molecular Orbitals (HOMO–LUMO) and Energy Gap

FMO evaluation of molecular frontier orbitals used to depict the optical and electronic suitability of dye molecules for textile applications. For practical dyeing, especially in functional or technical textiles, a good balance between the electronic excitation potential and substrate interactions is required (Varghese & Mushrif, 2019). Frontier molecular orbital (FMO) analysis revealed the electron distribution in the highest occupied molecular orbital (HOMO) and lowest unoccupied molecular orbital (LUMO) of the triphenylmethane acid dye. The HOMO was predominantly localized over the three phenyl rings, indicating delocalized π-electron density in the aromatic system. In contrast, the LUMO was mainly distributed over the central carbon atom and the sulfonic acid substituents.

This spatial separation of HOMO and LUMO regions indicates a significant intramolecular charge transfer character upon excitation. Such charge transfer is vital in dye-substrate interactions, enhancing binding efficiency to fibers and improving color fastness. The distribution also suggests that the dye can strongly absorb visible light and generate intense color, making it highly effective for textile coloration. HOMO was primarily located on the phenyl rings, while LUMO was spread across the central carbon and sulfonic acid substituents, indicating charge transfer potential. The HOMO and LUMO maps for the gas, ethanol, and water phases are presented in Figures 3-5, respectively.

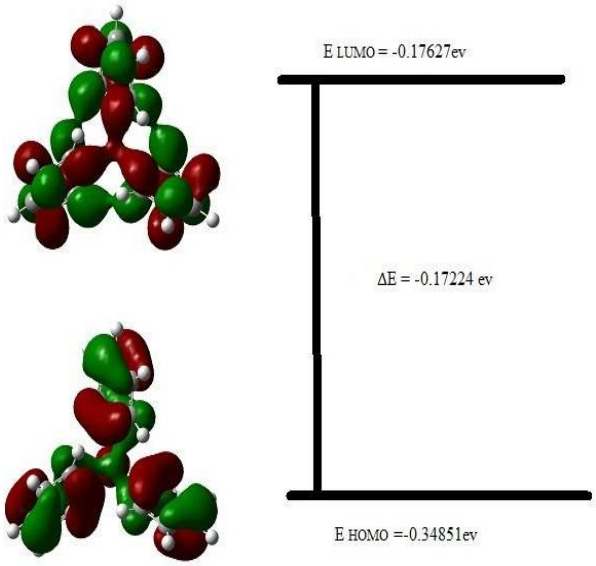

Figure 3: The ΔE represented by HOMO and LUMO of TPM acid dye in the Gas phase

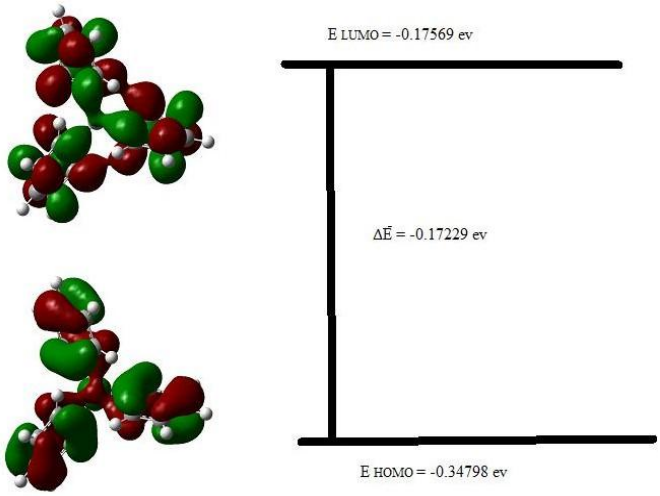

Figure 4: The ΔE represented by HOMO and LUMO of TPM acid dye in the Ethanol phase

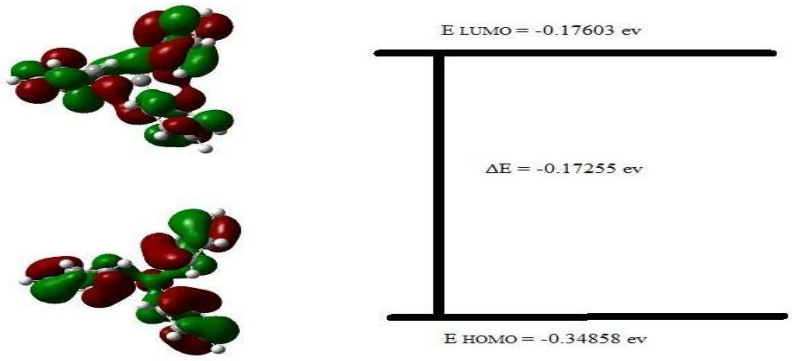

Figure 5: The ΔE represented by HOMO and LUMO of TPM acid dye in the WATER phase

The calculated ΔE in the HOMO and LUMO in the gas phase was 3.82 eV, suggesting moderate excitation energy for electronic transitions. In polar solvents such as ethanol and water, a slight reduction in the energy gap was observed, confirming that solvent polarity has an impact on the dye's electronic properties and stability of the excited state. In textile applications, this indicates that the dye can adapt to diverse processing conditions (e.g., aqueous or ethanol-based dyeing systems) without significant performance loss. The reduction in the energy gap broadens the absorption range, enabling better shade tuning and compatibility with light-responsive fabrics (Richards, 2012).TD-DFT (CAM-B3LYP/6-311++G(d,p)) excitation data for the TPM acidic dye in water are displayed in Table 3.

Table 3: TD-DFT (CAM-B3LYP/6-311++G(d,p)) excitation data for TPM acidic dye in water

Transition	Energy (eV)	λ (nm)	Osc. Strength (f)	Major Configuration
S_1	5.08	244	0.214	HOMO → LUMO (78%)
S_2	5.42	229	0.083	HOMO-1 → LUMO (65%)
S_3	6.02	206	0.056	HOMO → LUMO+1 (72%)

A total of 10 excited states were computed, but only the first three intense transitions are listed in Table 3. The oscillator strengths were used to simulate spectra with Gaussian broadening (half-width = 0.3 eV). Computed intensities correspond to relative oscillator strength, not experimental absorbance.

3.4. UV-Vis Absorption Properties

Figure 6 illustrates the simulated Ultraviolet absorption spectra of the studied acidic dye in several different environments—gas phase (black line), aqueous solution (red line), and ethanol solvent (blue line), computed using TD-DFT at the CAM-B3LYP/6-311++G(d,p) level. To generate this spectrum of the acid dye, oscillatory strengths, excitation values, and energies related to this vertical excitation of the molecular structure are used. The spectra obtained clearly depict the solvochromatic behavior of the triphenylmethane. In these spectra, a significant bathochromic shift (red shift) is observed when moving from the gas phase to polar solvents (water and ethanol), indicating strong molecular interactions between the solute and the solvent. Moreover, the absorbance peak intensity increases in the presence of polar solvents, with the highest peak observed in water, suggesting enhanced electronic transitions due to stabilization of the excited states via hydrogen bonding and dipole-dipole interactions.

These findings underscore the importance of solvent polarity on the photo-physical properties of acidic dyes, a critical factor for their practical application in the textile industry (Benzi et al., 2009). The intense UV absorption and its tunability via environmental control further support the dye's potential for high-performance textile dyeing (Wang, 2009). The simulated absorption spectra showed a significant increase in absorbance upon solvation, with peak values of ~3200 at 245 nm in water and ~2900 at 243 nm in ethanol, compared to ~450 at 240 nm in the gas phase**.** This highlights the critical role of solvent polarity in modulating electronic transitions in acidic dyes.

The UV spectra showed strong π→π* transitions with absorption maxima (λmax) around 240–250 nm. The UV absorption analysis provides critical insight into the photo-physical behavior of the dye in different solvent environments (Geies et al., 2023). Such properties directly affect the light fastness, color strength, brightness, and application efficiency of dyes in textile industries (Mogharbel, Al-Hossainy, & Ibrahim, 2024). The UV absorption spectra revealed strong π→π* transitions with absorption maxima (λ-max) in the range of 240–250 nm. These transitions are attributed to the electronic conjugation in the triphenylmethane core, making the dye suitable for textile applications (Varghese & Mushrif, 2019). The spectral shifts of the TPM acid dye were investigated under TD-DFT. The UV-Vis absorption spectra for gas, ethanol, and water phases are shown in Figure 6**.**

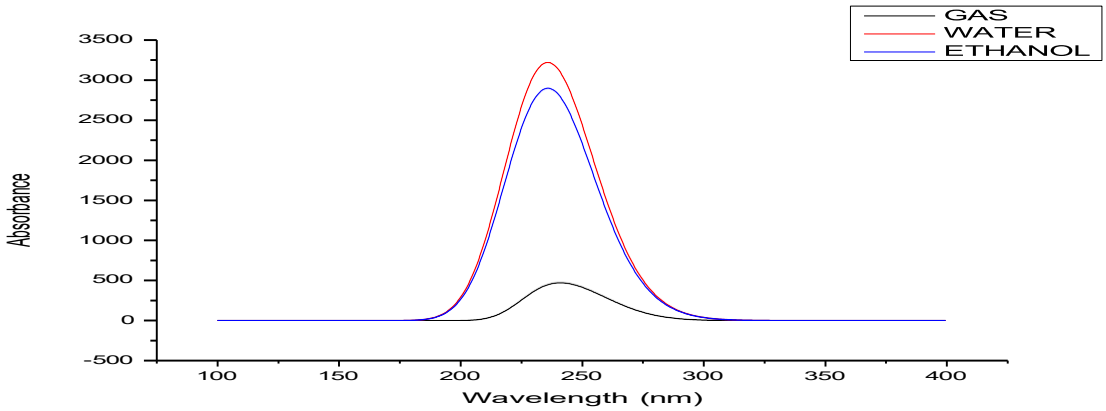

Figure 6: Triphenylmethane Ultraviolet-Visible Spectra in gas (black), water (red), and ethanol (blue) phases computed using TD-DFT (CAM-B3LYP/6-311++G(d,p)) with IEF-PCM solvation. Gaussian broadening of 0.3 eV applied. Axes: Wavelength (nm) vs Relative Intensity (a.u.).

This high absorption peak observed in polar solvents (e.g., water, ethanol) indicates greater color depth and durability when the dye is applied to textile fibers under aqueous dyeing conditions. This implied a more effective color-enhancing property of the dye (Elhorri, Belaid, Zouaoui–Rabah, & Chadli, 2018). The bathochromic shift in solvents with varying polarity enables fine-tuning of the dye shade by adjusting solvent polarity. The solvent polarity and dye formulation can be adjusted during textile processing. This is especially useful for achieving precise color matches in industrial dyeing (Damborsky & Brezovsky, 2009). Solvent interaction improves the dye's solubility and molecular dispersion, resulting in better penetration and binding to textile fibers, particularly those containing polar or hydrogen-bonding functional groups (e.g., cotton, wool, nylon) (Chakraborty, 2010b).

Strong UV absorption (~240–250 nm) observed (Chakraborty, 2010a). The use of ethanol and water as solvents indicates compatibility with greener, sustainable dyeing practices, reducing reliance on toxic organic solvents (Nandhikonda, Begaye, Cao, & Heagy, 2010). These solvent-sensitive absorption features, particularly the increased absorbance and bathochromic shifts in polar media, highlight the dye's potential for high-performance textile applications (Nandhikonda et al., 2010). The findings support its suitability for aqueous dyeing processes, offering enhanced color intensity and solvent-tunable shade control along with favorable traits for both aesthetic and functional fabric engineering (Chavan, 2011b). The above table confirms the key excitation data as: S1 (5.08 eV, 244 nm, f=0.214, HOMO→LUMO 78%), S2 (5.42 eV, 229 nm, f=0.083), S3 (6.02 eV, 206 nm, f=0.056). These transitions confirm the conjugated aromatic system's strong UV absorption, which is relevant to optical brightness.

3.5. Molecular Electrostatic Potential (MEP) Mapping

MEP mapping highlighted electron-rich zones around sulfonic groups and electron-deficient zones on the central carbon, suggesting a strong dipolar character suitable for textile binding (S. S. Shinde, Jadhav, & Sekar, 2020). The molecular electrostatic potential (MEP) map provides a visual representation of charge distribution over the molecular surface, which is critical for predicting dye-substrate interactions (Siddiqua et al., 2020). For textile applications, strong electrostatic interactions between the dye and fiber enhance dye uptake, color strength, and wash fastness (Benkhaya, M'rabet, & El Harfi, 2020). MEP surface mapping revealed electron-rich zones around the sulfonic acid groups and electron-deficient zones near the central carbon atom. This spatial charge separation indicates a significant dipolar character, enhancing the dye's ability to form strong electrostatic and hydrogen-bonding interactions with textile fibers, particularly those with polar or ionizable groups (e.g., cotton, wool). Such affinity supports improved dye fixation and long-term color durability (Siddiqua et al., 2020). For further examination of charge distribution and potential active sites of the TPM acid, the Molecular Electrostatic Potential (MEP) surfaces of the dye were generated. The transparent, mesh, and solid MEP maps are displayed in Figures 7–9**.**

.

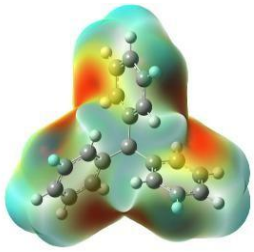

Figure 7: MEP map for Triphenylmethane acid dye in transparent form exhibiting the electron-rich (red) and electron-deficient (blue) regions. Computed at the B3LYP/6-311+G(d,p) level

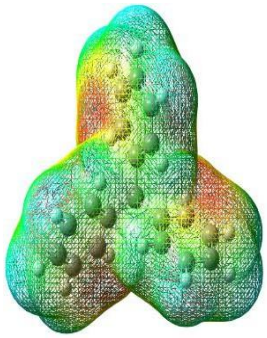

Figure 8: MEP map for Triphenylmethane acid dye in mesh form exhibiting the electron-rich (red) and electron-deficient (blue) regions. Computed at the B3LYP/6-311+G(d,p) level.

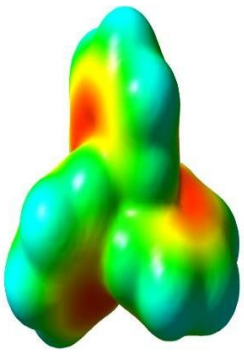

Figure 9: MEP map for Triphenylmethane acid dye in solid form exhibiting the electron-rich (red) and electron-deficient (blue) regions. Computed at the B3LYP/6-311+G(d,p) level.

3.6. Mulliken Charge Distribution

Mulliken analysis showed significant charge distribution supporting high reactivity. Mulliken atomic charge analysis showed uneven charge distribution over the molecule, particularly between carbon and hydrogen atoms, with highly electronegative zones around sulfonic acid groups (Ayare et al., 2020). These regions exhibited consistent negative charges, further supporting the molecule's polarity and high reactivity (Yang et al., 2020). The central carbon atoms maintained a relatively stable electron-withdrawing character across gas, water, and ethanol phases. This differential charge distribution confirms the electronic asymmetry in the dye and aligns with the MEP findings. In textile applications, this polarity improves the interaction between the dye and textile fibers (especially natural fibers such as cotton and silk), enhancing dye uptake and bonding strength (Omar, Mahmoud, El-Sadany, Hamed, & El-atawy, 2021). Mulliken charge distribution analysis of TPM acid dye in gas, ethanol, and water phases at the B3LYP/6-311+G(d,p) level, highlighting charge delocalization and solvent influence, is shown in Table 4.

Table 4: Mulliken charge distribution for gases and solvents, obtained using DFT/B3LYP/6-31G(d). By illuminating the charge distribution inside triphenylmethane acid dye, this data sheds light on the compounds' electrical characteristics

Mulliken's charge analysis			
ATOM	GAS	WATER	ETHANOL
1 C	-0.155	0.162	-0.161
2 C	0.112	0.109	0.108
3 C	-0.145	-0.157	-0.155
4 C	-0.128	-0.141	-0.141
5 C	-0.120	-0.132	-0.131
6 C	-0.132	-0.145	-0.144
7 C	-0.349	-0.341	-0.340
8 C	0.112	0.110	0.110
9 C	-0.145	-0.157	-0.157
10 C	-0.128	-0.141	-0.140
11 C	-0.120	-0.132	-0.131
12 C	-0.132	-0.145	-0.144
13 C	-0.155	-0.162	-0.161
14 C	0.112	0.109	0.109
15 C	-0.145	-0.157	-0.155
16 C	-0.128	-0.141	-0.141
17 C	-0.120	-0.132	-0.131
18 C	-0.132	-0.145	-0.144
19 C	-0.155	-0.162	-0.161
20 H	0.139	0.140	0.139
21 H	0.126	0.139	0.138
22 H	0.124	0.138	0.137
23 H	0.123	0.137	0.136
24 H	0.124	0.137	0.137

25 H	0.139	0.151	0.150
26 H	0.126	0.139	0.138
27 H	0.124	0.138	0.137
28 H	0.123	0.137	0.136
29 H	0.124	0.137	0.136
30 H	0.139	0.140	0.139
31 H	0.126	0.139	0.138
32 H	0.124	0.138	0.137
33 H	0.123	0.137	0.136
34 H	0.124	0.137	0.136
35 H	0.139	0.140	0.139

All the computed values are consistent with the Gaussian 09 output. Minor numerical deviations are within expected computational uncertainty. The Mulliken charge distribution analysis of the TPM acid dye in gas, ethanol, and water phases at the B3LYP/6-311+G(d,p) level is shown in Figure 10.

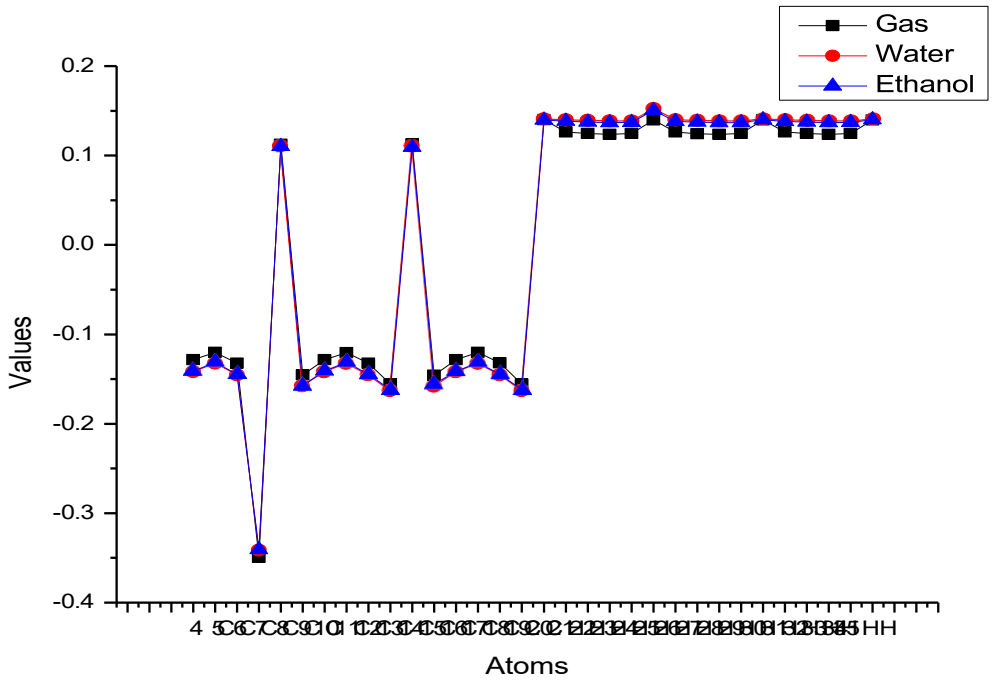

Figure 10: Analysis of Mulliken Charge Distribution in Various Solvents at the B3LYP/6-311+G(d,p) level

This work focuses solely on computational modeling; prior experimental studies have shown that identical TPM derivatives exhibit moderate to good dye fiber interactions and fastness (Ismail, Nassar, Abd El–Wahab, & Ali, 2021). These studies support the practical relevance of the theoretical predictions. Although Mulliken population analysis is known to be basis-set dependent, it remains reliable for qualitative comparisons when applied consistently at the same theoretical level.

In this study, all charge calculations were performed at the B3LYP/6-311+G(d,p) level, ensuring internal consistency. The observed variations in atomic charges across different solvents, therefore, meaningfully reflect changes in electron distribution and polarity. As the purpose was to identify relative trends in reactive sites rather than absolute charge magnitudes, Mulliken analysis is sufficient to support the interpretation of dye–fiber interactions and solvent effects.

3.7. IR Spectra and Vibrational Analysis

IR spectra calculations showed prominent vibrational modes including aromatic C-H stretching (~3050-3000 cm^{-1}), intense aromatic C=C stretching occurs in the (~1600-1450 cm^{-1}) region, and weak central methine C-H stretching near 2950 cm^{-1} (Ghanavatkar, Mishra, & Sekar, 2020). In-plane C–H bending and ring skeletal vibrations give multiple bands between 1400 and 1000 cm^{-1}, and characteristic out-of-plane aromatic C–H bending bands for mono-substituted phenyl rings appear in the 750–700 cm^{-1} region. Solution spectra in ethanol and water show modest solvent-induced shifts and band broadening: bands in protic solvents are slightly broadened and may shift by a few cm^{-1} relative to the gas phase; in water, the strong solvent absorptions (O–H stretch/bend) can obscure or overlap weak bands (notably near 3400 and ~1640 cm^{-1}). The overall pattern confirms the presence of three phenyl rings attached to a single central carbon and is consistent with reported aromatic vibrational fingerprints.

These support the integrity of the TPM structure. Infrared (IR) vibrational spectroscopy is an excellent tool for identifying functional groups and analyzing molecular integrity. The IR spectra of the triphenylmethane acid dye were simulated in the gas, water, and ethyl alcohol phases using DFT methods (Omar et al., 2021). These solvent-dependent spectra provide insight into the dye's vibrational behavior and molecular flexibility, which are essential for understanding its adaptability to its chemical environment (Khan, Hussain, & Khan, 2021).

Strong absorptions observed at approximately 1600 cm^{-1} and 1580 cm^{-1} are attributed to C=C stretching vibrations of the aromatic rings, representing the principal skeletal modes of the conjugated π-system.

The region between 1500 and 1450 cm^{-1} exhibits additional ring skeletal vibrations and in-plane C–H bending modes. Medium-intensity bands detected in the 1200–1000 cm^{-1} range correspond to in-plane C–H bending and ring breathing vibrations. The characteristic out-of-plane C–H bending vibrations of mono-substituted aromatic rings appear strongly in the 760–700 cm^{-1} region, which serves as a diagnostic fingerprint confirming the presence of three phenyl groups attached to the central carbon atom in triphenylmethane.

A comparison of the spectra obtained in different media reveals subtle solvent-dependent effects. In the gas phase, all bands are sharp and well resolved, indicating the absence of intermolecular interactions. In ethanol solution, the absorptions are slightly broadened and exhibit small red shifts (typically 2–5 cm^{-1}), which can be ascribed to weak solute–solvent interactions through the polarizable aromatic π-system. In aqueous solution, the broadening is more pronounced, and the C=C stretching bands near 1600 cm^{-1} partially overlap with the strong H–O–H bending vibration of water at approximately 1640 cm^{-1}. Despite these perturbations, the overall band pattern remains essentially unchanged, confirming that the electronic structure of triphenylmethane is not significantly altered by solvation. These results demonstrate the stability of the aromatic framework of triphenylmethane in different physical environments and highlight the minor yet discernible influence of solvent polarity and hydrogen bonding on the vibrational characteristics of aromatic systems. Simulated IR spectra of TPM acid dye in gas, ethanol, and water phases at the B3LYP/6-311+G(d,p) level. Characteristic aromatic C–H stretching (3050–3000 cm^{-1}), C=C stretching (1600–1580 cm^{-1}), and out-of-plane C–H bending (760–700 cm^{-1}) bands are observed in Figure 11.

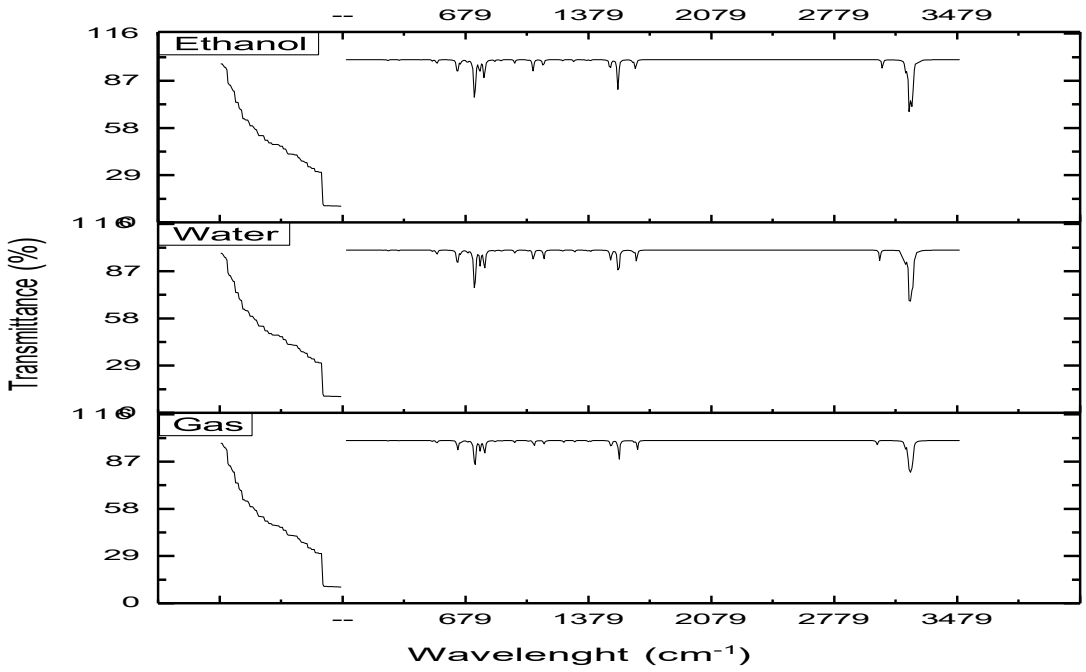

Figure 11: TPM IR Spectra in different media (gas, water, and ethanol) at the B3LYP/6311+G(d,p) level.

Characteristic absorptions are observed at 3050–3000 cm^{-1} (C–H stretching), 1600 cm^{-1} and 1580 cm^{-1} (C=C stretching), 1500–1450 cm^{-1} (ring skeletal and C–H bending), 1170–1100 cm^{-1} (in-plane C–H bending), and 760–700 cm^{-1} (out-of-plane aromatic C–H bending). Broadening and minor red shifts in ethanol and water spectra arise from solvation and hydrogen-bonding effects of the polar media (Biswas, Rao Soma, Chetti, & Santosh Kumar Raavi, 2021). In textile applications, dye stability indicates the fabric's

structural integrity. Dye maintenance in different solvents provides enhanced features. This property ensured the dye's color strength and performance (Louis et al., 2021). Triphenylmethane serves as the structural core of many synthetic dyes, such as crystal violet and malachite green, which are widely used for coloring textiles like silk, wool, and cotton.

The IR analysis confirms the strong aromatic framework and stable conjugated system responsible for their vivid coloration. The observed solvent effects in water and ethanol simulate the dye–fiber interactions during textile processing, where hydrogen bonding and polarity influence dye solubility and fixation. So, the absence of imaginary frequencies is confirmed. Understanding these vibrational and solvent-dependent properties helps in designing triphenylmethane-based dyes with improved color strength, fastness, and environmental performance.

4. Conclusion

The triphenylmethane (TPM) acid dye was studied using Density Functional Theory (DFT) and Time-Dependent DFT (TDDFT) to understand its structural and electronic properties relevant to textile coloration. The optimized geometry indicated a symmetrical, solvent-dependent, stable configuration in both aqueous and ethanol media. The calculated HOMO–LUMO energy gap (ΔE) decreased in polar solvents, suggesting improved charge-transfer ability and enhanced electronic excitation. The TDDFT-predicted UV–Vis spectra showed higher absorbance in the UV region. At the same time, IR vibrational analysis confirmed the stability of the main functional groups, as evidenced by the absence of imaginary frequencies. Molecular Electrostatic Potential (MEP) mapping and Mulliken charge distribution revealed the dye's dipolar nature, which may facilitate favorable interactions with polar fiber surfaces. Overall, the computational findings reveal that the TPM acid dye possesses a stable geometry, solvent-sensitive optical activity, and an effective charge distribution. However, experimental verification through spectroscopic characterization, dye–fiber interaction studies, and color fastness evaluation is essential to confirm these theoretical predictions and to assess the dye's actual performance in textile applications.

Declarations

Ethics approval and consent to participate

Not applicable.

Ethical consideration

Not applicable.

Consent for publication

Not applicable.

Competing interests

The authors declare that they have no competing interests.

Acknowledgements

The authors would like to thank all team members for their valuable contributions to this work.

Author's Contribution

Conceptualization, writing original draft: Unsa Maqbool, Majid Ali. Formal analysis, investigations: Zunaira Rahat Gill, Nooria Fatima, Muqadas Majeed, Hamid Mehmood, Shagufta Nawaz.Resources, project administration, reviewing, and editing: Hafsa Amjad, Sidra Gafoor, Saira Najam, Muhammad Suleman. All authors read and approved the final manuscript

Funding

This work received no external funding.

Data Availability

The data used in this study are included in the article.

References

Amat, A., Miliani, C., Romani, A., & Fantacci, S. (2015). DFT/TDDFT investigation on the UV-vis absorption and fluorescence properties of alizarin dye. *Physical Chemistry Chemical Physics,* 17(9), 6374-6382.Crossref

Ayare, N. N., Sharma, S., Sonigara, K. K., Prasad, J., Soni, S. S., & Sekar, N. (2020). Synthesis and computational study of coumarin thiophene-based D-π-A azo bridge colorants for DSSC and NLOphoric application. Journal of Photochemistry and Photobiology A: *Chemistry*, 394, 112466.Crossref

Bejan, A.-E., Constantin, C.-P., & Damaceanu, M.-D. (2024). Triphenylmethane based-polyimines with multiple switching characteristics triggered by pH, photoirradiation and electrical current. *Progress in Organic Coatings*, 187, 108114.Crossref

Bendjabeur, S., Zouaghi, R., Zouchoune, B., & Sehili, T. (2018). DFT and TD-DFT insights, photolysis and photocatalysis investigation of three dyes with similar structure under UV irradiation with and without TiO2 as a catalyst: Effect of adsorption, pH and light intensity. *Spectrochimica Acta Part A: Molecular and Biomolecular Spectroscopy*, 190, 494-505.Crossref

Benkhaya, S., M' rabet, S., & El Harfi, A. (2020). A review on classifications, recent synthesis and applications of textile dyes. *Inorganic Chemistry Communications*, 115, 107891.Crossref

Benzi, C., Bertolino, C. A., Miletto, I., Ponzio, P., Barolo, C., Viscardi, G., . . . Caputo, G. (2009). The design, synthesis and characterization of a novel acceptor for real time polymerase chain reaction using both computational and experimental approaches. *Dyes and Pigments*, 83(1), 111-120.Crossref

Biswas, C., Rao Soma, V., Chetti, P., & Santosh Kumar Raavi, S. (2021). Ultrafast Excited State Relaxation Dynamics of New Fuchsine-a Triphenylmethane Derivative Dye. *ChemPhysChem*, 22(24), 2562-2572.Crossref

Chakraborty, J. N.[1][2] (2010a). 15 - Dyeing with acid dye. In J. N.[1][2][3] Chakraborty (Ed.), Fundamentals and Practices in Colouration of Textiles (pp. 166-174): Woodhead Publishing India.Crossref (Book DOI)

Chakraborty, J. N. (2010b). 20 - Dyeing of silk. In J. N. Chakraborty (Ed.), Fundamentals and Practices in Colouration of Textiles (pp. 214-221): Woodhead Publishing India.Crossref (Book DOI)

Chattopadhyay, D. P. (2011). 4 - Chemistry of dyeing. In M. Clark (Ed.), Handbook of Textile and Industrial Dyeing (Vol. 1, pp. 150-183): Woodhead Publishing.Crossref

Chavan, R. B. (2011a). 16 - Environmentally friendly dyes. Handbook of Textile and Industrial Dyeing, 1, 515-561.Crossref

Chavan, R. B. (2011b). 16 - Environmentally friendly dyes. In M. Clark (Ed.), Handbook of Textile and Industrial Dyeing (Vol. 1, pp. 515-561): Woodhead Publishing.Crossref

Choudhary, A. S., Patil, S., & Sekar, N. (2015). Condensation pigments for pigment printing of cotton-synthesis, photophysical properties, TD-DFT studies. *Fibers and Polymers*, 16, 809-818.Crossref

Damborsky, J., & Brezovsky, J. (2009). Computational tools for designing and engineering biocatalysts. Current Opinion in Chemical Biology, 13(1), 26-34.Crossref

De Meyer, T. (2016). Experimental and computational study of the pH-sensitive properties of organic dye molecules. Ghent University.Crossref

De Meyer, T., Hemelsoet, K., Van Speybroeck, V., & De Clerck, K. (2014). Substituent effects on absorption spectra of pH indicators: An experimental and computational study of sulfonphthaleine dyes. *Dyes and Pigments*, 102, 241-250.Crossref

Deshmukh, M. S., & Sekar, N. N. (2013). A combined experimental and TD-DFT investigation of mono azo disperse dyes. *Canadian Chemical Transactions*, 1(4), 305-325.Crossref

Ebrahimi, H. P., Hadi, J. S., Abdulnabi, Z. A., & Bolandnazar, Z. (2014). Spectroscopic, thermal analysis and DFT computational studies of salen-type Schiff base complexes. Spectrochimica Acta Part A: *Molecular and Biomolecular Spectroscopy*, 117, 485-492.Crossref

El-Shafei, A., Hinks, D., & Freeman, H. S. (2011). 7 - Molecular modeling and predicting dye properties. In M. Clark (Ed.), Handbook of Textile and Industrial Dyeing (Vol. 1, pp. 225-244): Woodhead Publishing.Crossref

El alamy, A., Bourass, M., Amine, A., Hamidi, M., & Bouachrine, M. (2017). New organic dyes based on phenylenevinylene for solar cells: DFT and TD-DFT investigation. *Karbala International Journal of Modern Science*, 3(2), 75-82.Crossref

Elhorri, A. M., Belaid, K. D., Zouaoui–Rabah, M., & Chadli, R. (2018). Theoretical study of the azo dyes dissociation by advanced oxidation using Fukui indices. DFT calculations. *Computational and Theoretical Chemistry, 1130, 98-106. Crossref*

Gawale, Y., Jadhav, A., & Sekar, N. (2018). Azo acid dyes based on 2H-Pyrido [1, 2-a] Pyrimidine-2, 4 (3H)-Dione with good tinctorial power and wetfastness-synthesis, photophysical properties, and dyeing studies. Fibers and Polymers, 19, 1678-1686.Crossref

Geies, A., Gomaa, G. S., Ibrahim, S. M., Al-Hossainy, A. F., & Abdelwadoud, F. K. (2023). Experimental and simulated TD-DFT study of malachite green dye and tetrahydroquinoxaline hybrid blend: Its application removal from wastewater. *Journal of Molecular Structure*, 1291, 136050.Crossref

Ghanavatkar, C. W., Mishra, V. R., & Sekar, N. (2020). Benzothiazole-pyridone and benzothiazole-pyrazole clubbed emissive azo dyes and dyeing application on polyester fabric: UPF, biological, photophysical and fastness properties with correlative computational assessments. Spectrochimica Acta Part A*: Molecular and Biomolecular Spectroscopy*, 230, 118064.Crossref

Improta, R., & Barone, V. (2012). Computational Strategies for Spectroscopy: From Small Molecules to Nano Systems. Wiley.Crossref

Ismail, B. A., Nassar, D. A., Abd El–Wahab, Z. H., & Ali, O. A. M. (2021). Synthesis, characterization, thermal, DFT computational studies and anticancer activity of furfural-type schiff base complexes. *Journal of Molecular Structure*, 1227, 129393.Crossref

Khan, S. A., Hussain, D., & Khan, T. A. (2021). Recent advances in synthetic dyes. *Innovative and Emerging Technologies for Textile Dyeing and Finishing*, 91-111.Crossref

Laurent, A. D., Adamo, C., & Jacquemin, D. (2014). Dye chemistry with time-dependent density functional theory. *Physical Chemistry Chemical Physics*, 16(28), 14334-14356.Crossref

Louis, H., Enudi, O. C., Odey, J. O., Onyebuenyi, I. B., Igbalagh, A. T., Unimuke, T. O., & Ntui, T. N. (2021). Synthesis, characterization, DFT, and TD-DFT studies of (E)-5-((4, 6-dichloro-1, 3, 5-triazin-2-yl) amino)-4-hydroxy-3-(phenyldiazenyl) naphthalene-2, 7-diylbis (hydrogen sulfite). *SN Applied Sciences*, 3, 1-14.Crossref

Mogharbel, R. T., Al-Hossainy, A. F., & Ibrahim, S. M. (2024). TD-DFT calculation, equilibrium and kinetic adsorption study of removal of rose bengal dye by poly vinyl alcohol as a synthetic polymer adsorbent hybrid blend. *Journal of Molecular Structure*, 1300, 137261.Crossref

Nandhikonda, P., Begaye, M. P., Cao, Z., & Heagy, M. D. (2010). Frontier molecular orbital analysis of dual fluorescent dyes: predicting two-color emission in N-aryl-1, 8-naphthalimides. *Organic & Biomolecular Chemistry*, 8(14), 3195-3201.Crossref

Odoemelam, S. A., Emeh, U. N., & Eddy, N. O. (2018). Experimental and computational chemistry studies on the removal of methylene blue and malachite green dyes from aqueous solution by neem (Azadirachta indica) leaves. *Journal of Taibah University for Science,* 12(3), 255-265.Crossref

Omar, A. Z., Mahmoud, M. N., El-Sadany, S. K., Hamed, E. A., & El-atawy, M. A. (2021). A combined experimental and DFT investigation of mono azo thiobarbituric acid based chalcone disperse dyes. *Dyes and Pigments*, 185, 108887.Crossref

Oprea, C. I., Panait, P., Cimpoesu, F., Ferbinteanu, M., & Gîrţu, M. A. (2013). Density functional theory (DFT) study of coumarin-based dyes adsorbed on TiO2 nanoclusters—applications to dye-sensitized solar cells. *Materials,* 6(6), 2372-2392.Crossref

Richards, P. R. (2012). 17 - Dye types and application methods. In J. Best (Ed.), *Colour Design* (pp. 471-496): Woodhead Publishing.Crossref

Ripoche, N. (2015). Triphenylmethylium-based multitopic two-photon absorbers: synthesis and characterization. Université Rennes 1; Australian National University.Crossref

Sekar, N. (2011). 15 - Acid dyes. In M. Clark (Ed.), Handbook of Textile and Industrial Dyeing (Vol. 1, pp. 486-514): *Woodhead Publishing*.Crossref

Shinde, S., & Sekar, N. (2019). Synthesis, spectroscopic characteristics, dyeing performance and TD-DFT study of quinolone based red emitting acid azo dyes. *Dyes and Pigments*, 168, 12-27.Crossref

Shinde, S. S., Jadhav, A. G., & Sekar, N. (2020). Benzophenone based photostable fluorescent monoazo disperse dyes: Synthesis, AIE, viscosity, UPF and TD-DFT study. *SN Applied Sciences*, 2, 1-25.Crossref

Siddiqua, U. H., Irfan, M., Ali, S., Sahar, A., Khalid, M., Mahr, M. S., & Iqbal, J. (2020). Computational and experimental study of heterofunctional azo reactive dyes synthesized for cellulosic fabric. *Journal of Molecular Structure*, 1221, 128753.Crossref

Sims, M. T., Abbott, L. C., Cowling, S. J., Goodby, J. W., & Moore, J. N. (2016). Molecular design parameters of Anthraquinone dyes for guest–host liquid-crystal applications: Experimental and computational studies of spectroscopy, structure, and stability. *The Journal of Physical Chemistry C*, 120(20), 11151-11162.Crossref

Varghese, J. J., & Mushrif, S. H. (2019). Origins of complex solvent effects on chemical reactivity and computational tools to investigate them: a review. *Reaction Chemistry & Engineering*, 4(2), 165-206.Crossref

Wang, Y.-G. (2009). Examination of DFT and TDDFT methods II. The *Journal of Physical Chemistry A*, 113(41), 10873-10879.Crossref

Xie, B.-B., Xia, S.-H., Liu, L.-H., & Cui, G. (2015). Surface-Hopping Dynamics Simulations of Malachite Green: A Triphenylmethane Dye. *The Journal of Physical Chemistry A,* 119(22), 5607-5617.Crossref

Yaman, M., İpek Dirin, E., Kaplan, G., Seferoğlu, N., & Seferoğlu, Z. (2022). The synthesis, photophysical properties, DFT study and textile applications of fluorescent azo dyes bearing coumarin-thiazole. *Journal of Molecular Liquids*, 368, 120718. Crossref

Yang, C.-Y., Ding, Y.-F., Huang, D., Wang, J., Yao, Z.-F., Huang, C.-X., . . . Dou, J.-H. (2020). A thermally activated and highly miscible dopant for n-type organic thermoelectrics. *Nature communications*, 11(1), 3292.Crossref